Please cite this article in press as: Weber et al., Mitotic Position and Morphology of Committed Precursor Cells in the Zebrafish Retina Adapt to Architectural Changes upon Tissue Maturation, Cell Reports (2014), http://dx.doi.org/10.1016/j.celrep.2014.03.014

Cell Reports
Report

Mitotic Position and Morphology of Committed Precursor Cells in the Zebrafish Retina Adapt to Architectural Changes upon Tissue Maturation

Isabell P. Weber,[1] Ana P. Ramos,[1] Paulina J. Strzyz,[1] Louis C. Leung,[1] Stephen Young,[2,3] and Caren Norden[1,*]
[1]Max Planck Institute of Molecular Cell Biology and Genetics, Pfotenhauerstraße 108, 01307 Dresden, Germany
[2]RIKEN Quantitative Biology Center, Osaka 565-0874, Japan
[3]Department of Biological Sciences, Osaka University, Osaka 560-0043, Japan
*Correspondence: norden@mpi-cbg.de
http://dx.doi.org/10.1016/j.celrep.2014.03.014

SUMMARY

The development of complex neuronal tissues like the vertebrate retina requires the tight orchestration of cell proliferation and differentiation. Although the complexity of transcription factors and signaling pathways involved in retinogenesis has been studied extensively, the influence of tissue maturation itself has not yet been systematically explored. Here, we present a quantitative analysis of mitotic events during zebrafish retinogenesis that reveals three types of committed neuronal precursors in addition to the previously known apical progenitors. The identified precursor types present at distinct developmental stages and exhibit different mitotic location (apical versus nonapical), cleavage plane orientation, and morphology. Interestingly, the emergence of nonapically dividing committed bipolar cell precursors can be linked to an increase in apical crowding caused by the developing photoreceptor cell layer. Furthermore, genetic interference with neuronal subset specification induces ectopic divisions of committed precursors, underlining the finding that progressing morphogenesis can effect precursor division position.

INTRODUCTION

Generating the complex 3D arrangements of tissues and organs poses multiple challenges to cells. They have to adjust their morphology, division state (proliferation versus differentiation), and position within the tissue according to cellular function. Striking examples of cellular rearrangement occur during the development of the central nervous system. In the retina, morphogenetic changes lead to the highly organized layered structure of the mature organ. Correct retinal development is crucial for visual perception of the environment and therefore of major importance for the organism.

The retina develops from a pseudostratified neuroepithelium into a laminated tissue in which neuronal subtypes are arranged in distinct layers. In general, pseudostratified neuroepithelia consist of elongated progenitors that are highly polarized along their apicobasal axis and that undergo apical division (Lee and Norden, 2013). In the retina, such apical progenitors are multipotent and ultimately give rise to all retinal cell types (Agathocleous and Harris, 2009; He et al., 2012). It was proposed that apical progenitors pass through different competence states during retinogenesis, thereby giving rise to distinct lineages (Livesey and Cepko, 2001). Although we now know that some plasticity exists for fate choices of equipotent progenitors (Gomes et al., 2011; He et al., 2012), the following birth order of retinal neurons has been suggested in zebrafish. First, retinal ganglion cells (RGCs) are born that migrate to and later occupy the most basal retinal layer. RGCs feature long axons that form the optic nerve and thereby transmit visual information into the brain. Next, and overlapping with RGCs, the most apically located cone photoreceptors (PRs) are born. Cone PRs, together with late-born rod PRs, form the most apical layer of the retina, the outer nuclear layer (ONL), or PR layer, responsible for light collection. Slightly later in development, interneurons that inhabit the inner nuclear layer (INL; the layer between the PR layer and the RGC layer) arise, namely horizontal cells (HCs), amacrine cells (ACs), and bipolar cells (BCs) (He et al., 2012). Two nucleus-free plexiform layers in which synaptic connections are established separate the three nuclear layers in the mature retina: the outer plexiform layer (OPL) and the inner plexiform layer (IPL) (Sernagor et al., 2006). It was long assumed that terminally dividing apical progenitors give rise to all retinal neurons, which subsequently migrate to their final laminar position, polarize, and integrate into the neuronal network (Turner et al., 1990). However, taking the neuronal birth order and the inhomogeneity of retinal layer formation into account, it becomes clear that already early in retinogenesis, tissue changes and morphogenetic obstacles emerge. These could influence later stages of retinogenesis. In particular, the fact that the most apical layer in which mitosis of multipotent progenitors is supposed to take place becomes inhabited by PRs early in development raises the question of whether this influences divisions at the apical surface. The discovery of committed HC precursors dividing at basal positions during zebrafish and chick retinal development revealed that not all retinal progenitor divisions are restricted to the apical surface (Boije et al., 2009; Godinho et al., 2007). These observations

Please cite this article in press as: Weber et al., Mitotic Position and Morphology of Committed Precursor Cells in the Zebrafish Retina Adapt to Architectural Changes upon Tissue Maturation, Cell Reports (2014), http://dx.doi.org/10.1016/j.celrep.2014.03.014

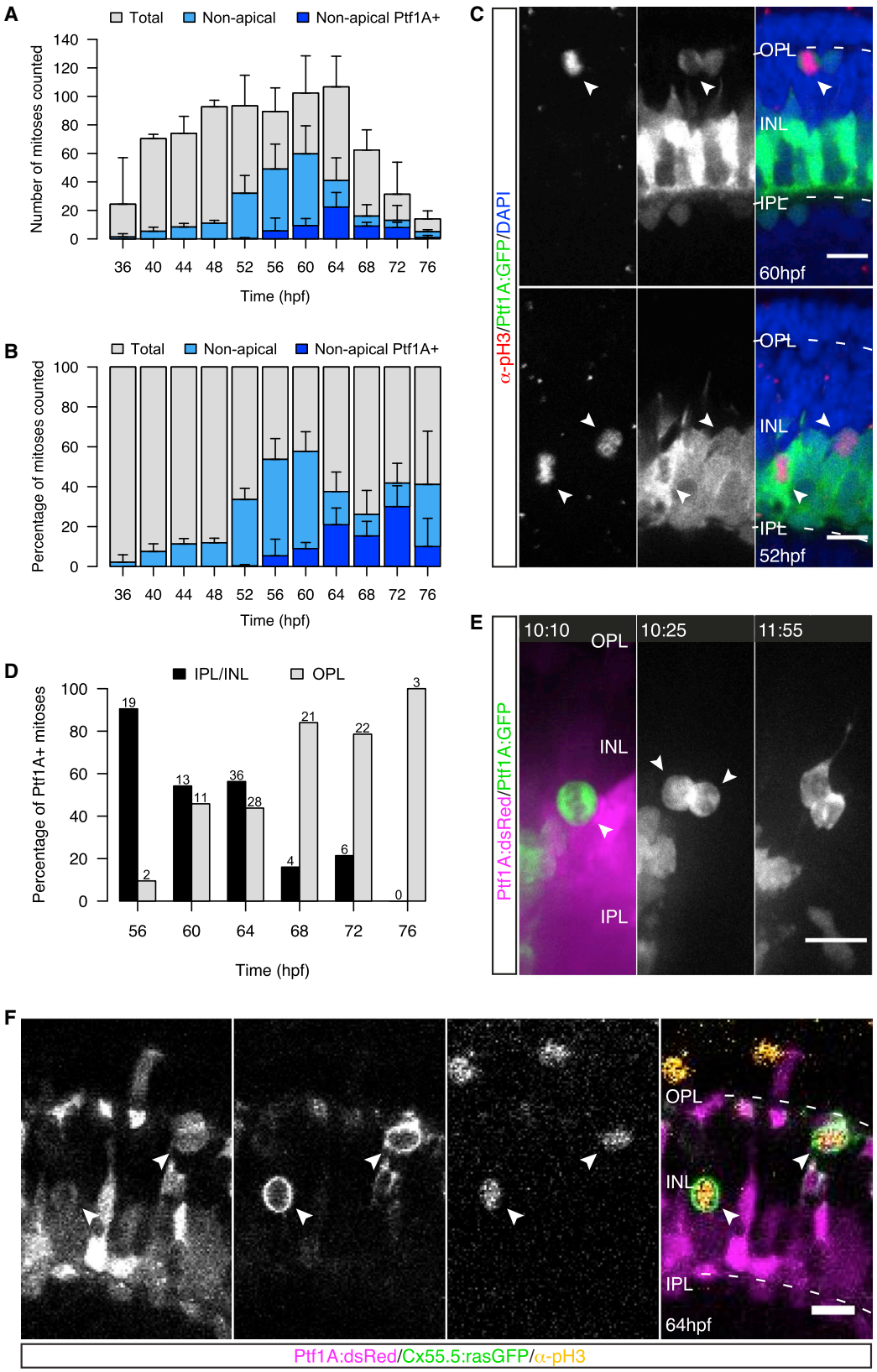

(legend on next page)

raise three important questions. (1) Do additional pools of committed retinal precursors exist? (2) If so, when during retinogenesis do they emerge and where do they divide? (3) Do morphogenetic changes accompanying retinogenesis and the occurrence of tissue obstacles influence precursor pools and their mitotic positions?

In this study, we address these questions by systematically analyzing the occurrence and contribution of committed precursor divisions during zebrafish retinal development. Performing immunostainings and live imaging, we reveal three classes of symmetrically dividing committed neuronal precursors. They appear at different stages of late retinal development between 48 and 76 hours postfertilization (hpf); BC and HC precursors divide at different nonapical positions and display distinct morphologies. Additionally, apically dividing PR precursors emerge that exhibit short, rectangular morphology different from that of apical progenitors. Finally, we present evidence that the shift of BC precursor divisions to nonapical positions can be linked to apical crowding.

RESULTS

Three Phases of Mitotic Activity Occur during Zebrafish Retinogenesis at Different Apicobasal Locations

The discovery of basally dividing committed HC precursors (Godinho et al., 2007; Boije et al., 2009) demonstrated a need to reevaluate retinal precursor types and their mitotic positions. We therefore analyzed cell divisions in the central retina between 36 hpf, the time when retinal neurogenesis in zebrafish starts, and 76 hpf, when the retina becomes functional and only few mitotic events still occur (He et al., 2012). Embryos were fixed in 4 hr intervals and stained against the late G2/M phase marker phosphohistone-H3 (pH3). pH3-positive (from here on pH3+) cells were analyzed in sagittal optical sections of the central/middle part of the retina as defined by He et al. (He et al., 2012). Depending on the position of pH3 signal, cells were defined as apical when dividing at the apical surface or as nonapical when occurring more than a full nuclear length away from the apical surface.

Our quantification revealed three phases of mitotic activity during retinal development. First, at early developmental stages between 36 and 48 hpf, divisions occurred almost exclusively at the apical surface, most likely representing divisions of apical neuroepithelial progenitors (Figures 1A and 1B). Nonapical divisions became more frequent after 48 hpf, and their relative as well as absolute abundance rose until 60 hpf (Figures 1A and 1B, light blue bars). At this point, nonapical mitoses outnumbered apical mitoses (Figures 1A and 1B). After 64 hpf, mitotic events in the central retina became less frequent. At these late developmental stages, nonapical divisions represented a relatively stable proportion (~30%–40%) of total divisions (Figure 1B) and the amount of apical divisions rose again (Figures 1A and 1B).

Nonpolar Horizontal Cell Precursors Divide at Multiple Basal Locations

Nonpolar (i.e., not featuring apical or basal processes) committed HC precursors were described previously to divide at nonapical locations adjacent to the OPL during zebrafish development (Godinho et al., 2007). To investigate whether these precursors account for the entire proportion of nonapically dividing cells in Figures 1A and 1B, we quantified their onset and prevalence using a transgenic line expressing Ptf1A promoter-driven GFP (Jusuf et al., 2012; Leung et al., 2011) (Figure 1C). The transcription factor Ptf1A is involved in determining inhibitory cell lineages and expressed in all ACs and HCs (Godinho et al., 2007; Jusuf et al., 2011). Analyzing the contribution of pH3+/Ptf1A-positive (from here on Ptf1A+) cells to the proportions of apically and nonapically dividing cells from Figures 1A and 1B revealed that Ptf1A+ cells accounted only for a subset of nonapical divisions observed (Figures 1A and 1B, dark blue bars). Ptf1A+ cells never divided apically and nonapical divisions of Ptf1A+ cells started to occur at 56 hpf. They were most abundant around 64 hpf and decreased in frequency toward the end of retinogenesis (Figures 1A and 1B). Ptf1A+ divisions were observed adjacent to the OPL (Figure 1C, top) but also in more basal regions of the INL (Figure 1C, bottom, and Figure 1E). Interestingly, at 56 hpf, Ptf1A+ divisions occurred almost exclusively in the basal INL and only from 60 hpf on did the proportion of divisions near the OPL increase. While OPL divisions became more abundant over time, the proportion of INL/IPL divisions decreased until 76 hpf (Figure 1D). Because Ptf1A labels HCs as well as ACs, these results raised the possibility that ACs were born from basal divisions in the INL. We generated an HC-specific transgenic line using promoter elements of connexin Cx55.5 driving rasGFP (Godinho et al., 2007; Shields et al., 2007) and performed live imaging and pH3 staining of Ptf1A:dsRed/Cx55.5:rasGFP embryos. All Ptf1A+ divisions in the INL were also Cx55.5 positive (from here on, Cx55.5+), thus representing committed HC precursors (Figure 1F; Movie S1). All HC precursors were nonpolar (Figure 1F; Movie S1; Figure S1A) and lost their preference for division angles perpendicular to the apical

Figure 1. HC Precursors Divide at Multiple Positions but Do Not Account for All Nonapical Divisions

(A) Total number of pH3+ cells (gray), nonapically dividing cells (light blue), and Ptf1A+ nonapically dividing cells (dark blue) counted at each time point/embryo. Error bars represent SD; n = 2–6 embryos per time point.

(B) Data from (A) as percentage of all counted mitoses. Error bars represent SD.

(C) Ptf1A:GFP (green) embryos stained for pH3 (red) and DAPI (blue). Ptf1A+/pH3+ cells are found adjacent to the OPL (top, arrows) and within the AC layer (bottom, arrows).

(D) Quantification of the location of Ptf1A+/pH3+ cells as percentage of pH3+ cells. Numbers on top of bars indicate number of dividing cells counted. n = 3 embryos/time point, pooled.

(E) INL division of a Ptf1A:GFP cell gives rise to two Ptf1A+ daughters (arrows). Time in hr:min. Imaging started at 46 hpf.

(F) pH3 staining (yellow) of a Ptf1a:dsRed/Cx55.5:rasGFP (magenta/green) embryo. All cells in the INL and adjacent to the OPL immunoreactive for pH3 express Ptf1A:dsRed and Cx55.5:rasGFP (arrows).

Scale bars represent 10 μm. See also Figure S1 and Movie S1.

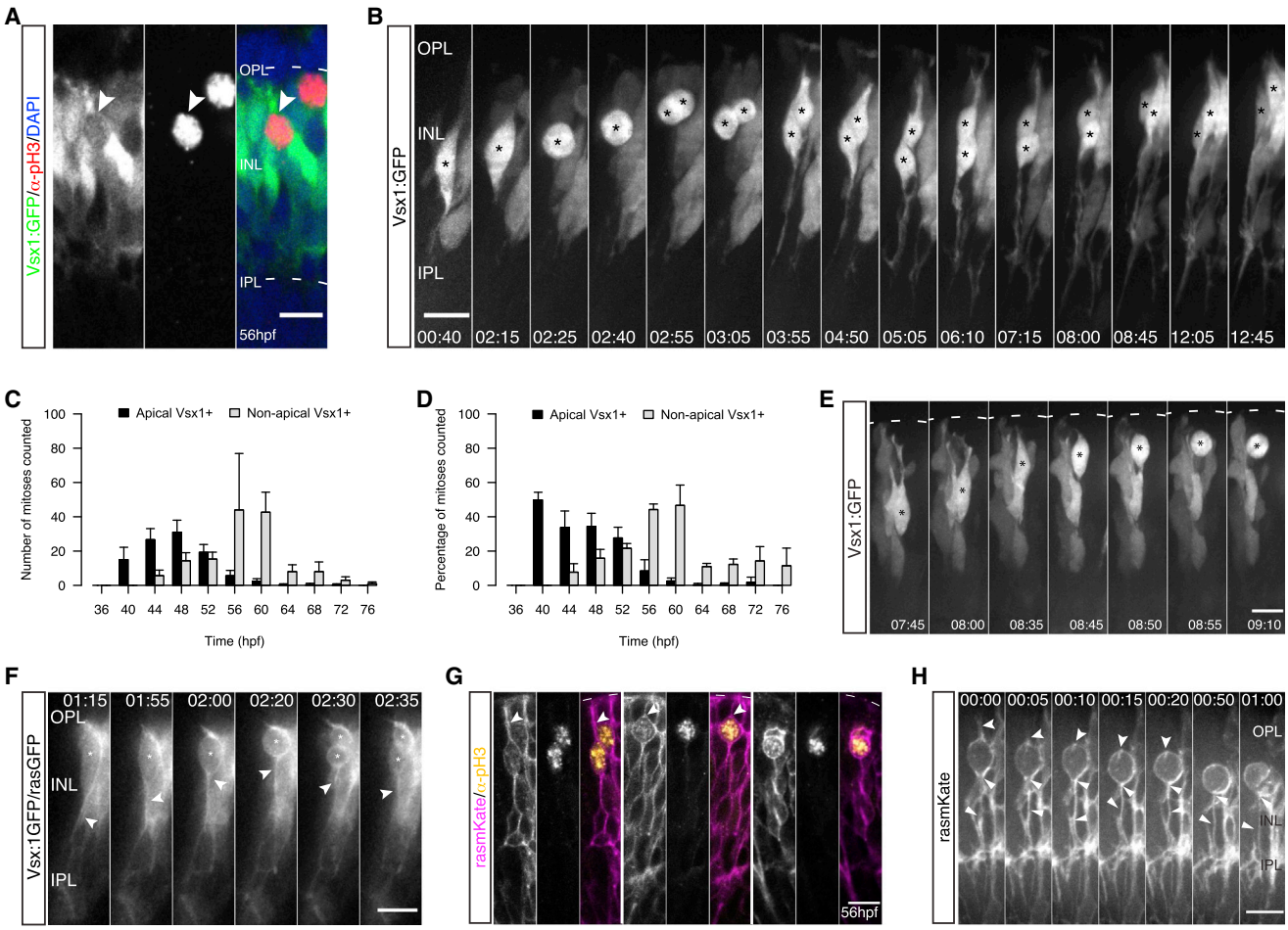

Figure 2. Nonapically Dividing Monopolar Vsx1+ Precursors Give Rise to Two Bipolar Cells

(A) pH3 (red) and DAPI staining (blue) in a Vsx1:GFP (green) embryo. pH3+/Vsx1+ cells are observed in the INL (arrows).

(B) Two Vsx1+ cells arise from a nonapically dividing Vsx1:GFP cell, align in the INL, and feature BC morphology (asterisk) (from Movie S2). Time hr:min. Imaging started 50 hpf.

(C) Time course showing counts of apically and nonapically dividing Vsx1+ cells/embryo (36–76 hpf; 4 hr intervals). Error bars represent SD; n = 2–3 embryos per time point.

(D) Data from (C) as percentage of all counted mitoses. Error bars represent SD.

(E) Vsx1:GFP cell bodies undergo IKNM-like movement prior to subapical division (asterisk). Time in hr:min. Imaging started at 48 hpf.

(F) A transplanted Vsx1:GFP/rasGFP cell divides adjacent to the OPL (asterisk), featuring a basal process before, during, and after mitosis (notched arrows). Time in hr:min. Imaging started at 52 hpf.

(G) Embryos mosaically injected with rasmKate RNA (magenta) stained for pH3 (yellow). Cells are attached apically in late G2 (left, arrows). An apical process is present at the beginning of cell rounding (arrows, middle) but lost upon entry into mitosis (right).

(H) Time-lapse of an embryo mosaically injected with rasmKate. Upon onset of cell rounding, an apical process can be observed (notched arrows), which is lost upon entry into mitosis. Filled arrows point toward basal process; from Movie S3. Time in hr:min. Imaging started at 56 hpf.

Scale bars represent 10 μm. See also Figure S1.

side (27% perpendicular, 27% oblique, and 46% horizontal to the apical side; n = 15).

Bipolar Cells Are Born from Nonapical Symmetric Divisions of Monopolar Precursors

These findings do not explain the majority of nonapical divisions observed between 40 and 76 hpf (Figures 1A and 1B). Thus, we set out to explore the identity of the remaining nonapically dividing cells. Nonapically dividing Ptf1A-negative cells were mainly observed in the INL occurring at developmental stages at which BCs are born (He et al., 2012). Hence, we speculated that these cells correspond to BC precursors. We performed pH3 staining in a transgenic line expressing Vsx1 promoter-driven GFP because Vsx1 is expressed in most BC subtypes (Passini et al., 1997; Vitorino et al., 2009). Analysis of Vsx1:GFP embryos confirmed that pH3+/Vsx1-positive (from here on, Vsx1+) cells are recurrently found between the OPL and IPL (Figure 2A). Furthermore, the combination of cell transplantations and live imaging showed that between 48 and 56 hpf, Vsx1+ precursors frequently divided nonapically, giving rise to two

Vsx1+ cells (Figure 2B; Movie S2). In cases in which we were able to follow such Vsx1+ daughter cells, both cells adopted BC morphology and integrated into the INL (Figure 2B; Movie S2).

For quantitative evaluation of BC precursor divisions, a time course as outlined above was performed using Vsx1:GFP embryos. At 40 hpf, Vsx1+ divisions occurred exclusively at the apical surface (Figure 2C; Figures S1B–S1E). From 44 to 56 hpf, nonapical Vsx1+ divisions became more abundant (Figures 2C and 2D; Figures S1B–S1E). At 44 hpf, they marked a small fraction (~8%) of all retinal mitoses but represented ~47% of all mitotic events analyzed at 56 and 60 hpf (Figures 2Cs and 2D; Figures S1D and S1E).

Next, we explored the morphology of nonapically dividing BC precursors. Interestingly, the cell bodies of these cells underwent a movement toward the apical side prior to division reminiscent of interkinetic nuclear migration (IKNM) (Figure 2E) (Lee and Norden, 2013). However, before reaching the apical side, they entered mitosis and divided without preference for perpendicular division angles (31% perpendicular, 22% oblique, and 47% horizontal to the apical side; n = 36). Because cytosolic expression of Vsx1-driven GFP did not allow for the resolution of cellular processes, we injected RNA of plasma membrane-localized rasGFP into Vsx1:GFP embryos. Transplanting Vsx1:GFP/rasGFP cells into control background revealed that nonapically dividing Vsx1+ cells maintain a basal process during division (Figure 2F; Movie S3). Mosaic RNA injections of plasma membrane-localized rasmKate combined with staining for pH3 (Figure 2G) as well as live imaging of rasmKate-injected embryos further showed that nonapical Vsx1+ precursors lose their apical process just upon entry into mitosis (Figure 2H; Movie S3).

Late Apical Divisions Represent Committed Photoreceptor Cell Precursors

Committed BC and HC precursors together explain the nonapical mitoses observed between 52 and 72 hpf. Interestingly, though, once nonapical divisions already started to decrease, we saw a second rise of apical divisions between 60 and 72 hpf (Figure 1A). A recent study reported a pool of apically dividing committed cone PR precursors (Suzuki et al., 2013), and we asked whether and to what extent such precursors account for the late apical mitotic events seen. pH3 staining of an Ath5:gapGFP line to label cone PRs (Ma et al., 2004; Poggi et al., 2005) confirmed that apical Ath5-positive (from here on, Ath5+) divisions exist at late stages of retinogenesis (Figure 3A; Figure S2A), presenting a third pool of committed retinal precursors. Ath5+ PR precursor divisions constitute the vast majority of all apical divisions between 60 and 76 hpf (Figure S2B). Cells undergoing apical divisions at these stages are not elongated like apical progenitors but display short, rectangular, PR-like morphology before and after division (Figure 3B; Movie S4).

Apical Space Constraints Can Shift Mitotic Figures to Nonapical Locations

Next, we explored the question of why mitotic positions of BC precursors relocate from apical to nonapical locations between 48 and 56 hpf (Figure 2C and 2D). We noticed that the developmental time window at which repositioning of mitoses toward nonapical locations occurred coincided with PR layer development (Hu and Easter, 1999; Perkins and Fadool, 2010). To determine whether a correlation between PR layer emergence and the repositioning of BC precursor mitoses exists, we stained Ath5:gapRFP+/Vsx1:GFP+ embryos for pH3. Apical Vsx1+ divisions occurred exclusively in regions in which PRs did not yet inhabit the most apical side (Figure 3C, top). Conversely, nonapical Vsx1+ divisions were seen only in regions in which PRs already occupied the apical surface (Figure 3C, bottom). Live imaging of Vsx1:GFP/Ath5:gapRFP embryos clearly showed that at stages at which the PR layer has not yet developed, nuclei of Vsx1+ cells reach the apical side and undergo apical division (Figure 3D, top; Movie S5). In contrast, in the same embryo, upon PR layer establishment, Vsx1+ cell bodies cannot reach the apical side, leading to nonapical divisions (Figure 3D, bottom; Movie S5). When we analyzed the distribution of mitotic location along the apicobasal axis between 48 and 72 hpf, we observed that the relative frequency of subapical divisions rose after 56 hpf (Figure 3E, left). Strikingly, the increasing refinement and separation of the apical and nonapical mitotic peaks correlated with the formation of the OPL (Figure 3E).

Together, these results suggest that maturing PRs at the apical side act as a spatial hindrance that prevents cell bodies of Vsx1+ precursors from reaching apical positions, thereby shifting mitotic figures to nonapical locations.

To test whether apical space constraints in general lead to the repositioning of mitotic figures, we treated 28-hpf-old embryos with the Polo-like kinase 1 inhibitor BI2536 (Lénárt et al., 2007), thereby arresting neuroepithelial progenitors in mitosis. Cells blocked in M phase accumulated apically and led to congestion at the apical side 5 hr after drug treatment (Figure 4A, 8 hr 50 min; Movie S6). Although rounded cells arrested in mitosis eventually fully occupied the apical space, further nuclei traveled apically to undergo cell division. Strikingly, this resulted in additional layers of mitotic cells beneath the most apical layer at positions comparable to those of nonapically dividing BC precursors (Figure 4A, 11 hr 5 min; Movie S6; Figures 2A and 2B). We next explored whether such repositioned cells lose their apical process upon entry into mitosis as seen for the sub-apically dividing BC precursors. In BI2536-treated embryos injected with rasmKate and centrin-GFP to follow centrosome movement and spindle formation, the centrosome traveled toward the nucleus and met the nucleus nonapically. Detachment of the apical process only occurred subsequently (Figure 4B). This resembles what is observed for BC precursors.

Bipolar Cell Precursors Keep Dividing at Apical Locations in Scenarios in which Photoreceptor Cell-Layer Formation Is Compromised

Our observations suggest that PR layer emergence is involved in the shift of BC precursor divisions to nonapical positions. However, to test that a real causality and not just a correlation between these two events exists, we designed an experiment to interfere with PR layer formation. A previous study indicated that a combination of the *dynactin-1* mutant *mok* with the *ath5* mutant *lakritz* leads to disturbed PR layer formation (Del Bene et al., 2008). Indeed, injecting a morpholino mix against *dync1h1* (Insinna et al., 2010), *ath5* (Pittman et al., 2008), and *p53* (to suppress apoptosis; Randlett et al., 2013) into

Please cite this article in press as: Weber et al., Mitotic Position and Morphology of Committed Precursor Cells in the Zebrafish Retina Adapt to Architectural Changes upon Tissue Maturation, Cell Reports (2014), http://dx.doi.org/10.1016/j.celrep.2014.03.014

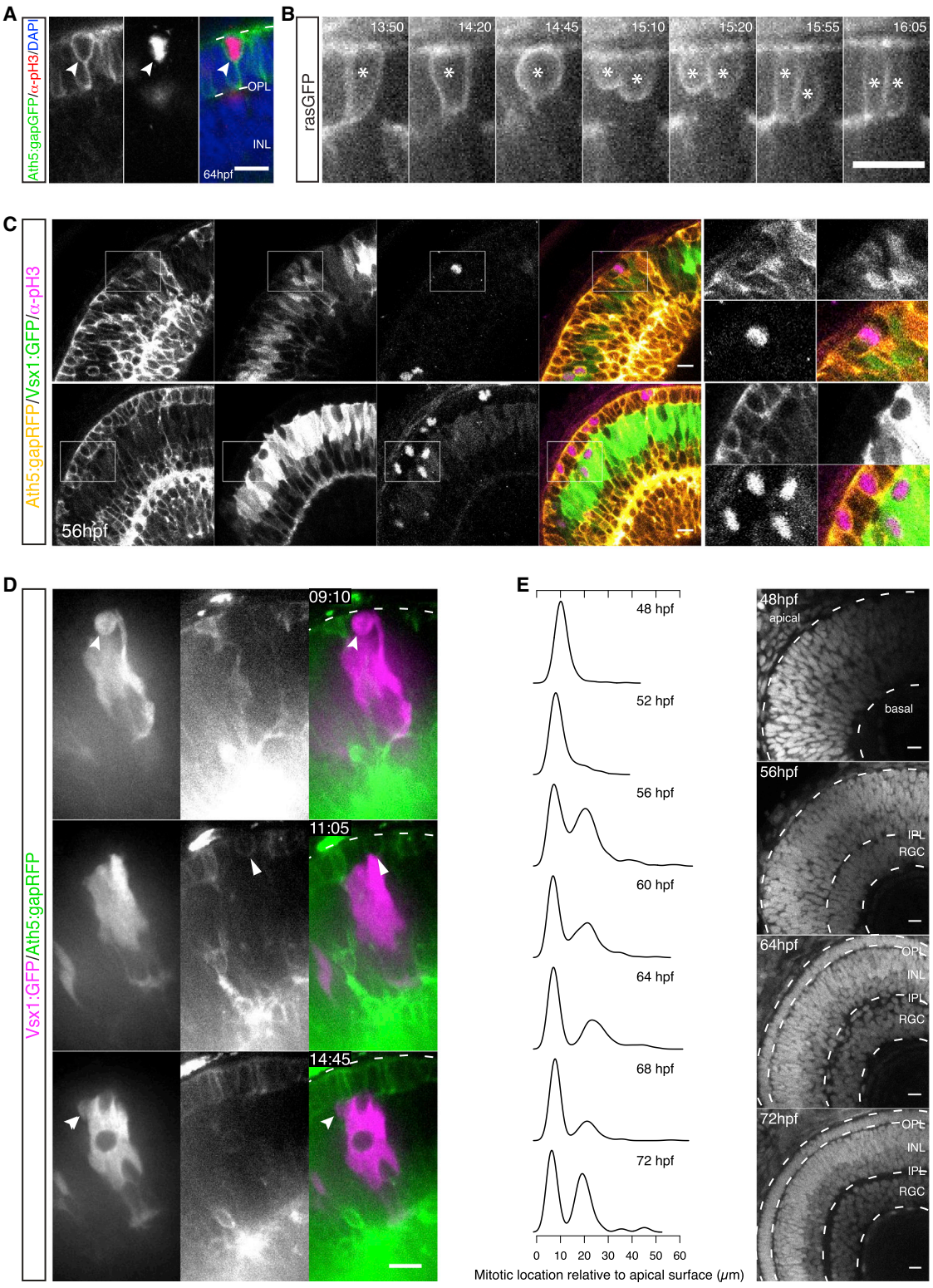

Figure 3. Emergence of the Photoreceptor Cell Layer Leads to Repositioning of Bipolar Cell Precursor Divisions

(A) A pH3+/Ath5+ (red/green) cell within the PR layer (DAPI counterstaining in blue).

(B) A rasGFP+ cell (asterisk) undergoes division within the PR layer, giving rise to two daughters with PR-like morphology (from Movie S4). Time in hr:min. Imaging started at 50 hpf.

(legend continued on next page)

Vsx1:GFP/Ath5:gapRFP embryos resulted in retinae in which the continuity of the PR layer was interrupted by patches of Vsx1+ cell bodies reaching the apical side (Figure 4C). Strikingly, examination of pH3 staining in these transgenic morphants revealed that Vsx1+ cells divided apically in such PR-free patches, while Vsx1+ cells divided nonapically in adjacent regions with an intact PR layer (Figure 4D; Figure S3A). Together, these experiments argue that the development of apical constraints plays a role in the repositioning of cell divisions to nonapical locations.

Ectopic Basal Mitoses Are Involved in the Retention of Retinal Tissue Architecture upon Interference with the Specification of Neuronal Subtypes

The zebrafish retina is capable of compensating the loss of specific neuronal subtypes by the overproduction of other retinal neurons, thereby retaining proper lamination (Kay et al., 2001; Jusuf et al., 2012; Randlett et al., 2013). Thus, we asked if localized ectopic divisions are part of such compensation. To test this possibility, we used an *ath5* morpholino (Pittman et al., 2008), because Ath5 downregulation interferes specifically with RGC fate determination, resulting in RGC loss (Kay et al., 2001). In Ptf1A:GFP embryos injected with *ath5* morpholino, not RGCs but Ptf1A+ cells inhabit the most basal region of the retina (Figure 5A). Interestingly, examination of pH3 staining in such transgenic *ath5* morphants at 64 hpf showed that mitotic Ptf1A+ cells frequently occurred at locations close to the inner limiting membrane (ILM), which in controls represent the RGC layer (Figure 5B). Quantification of control versus *ath5* morphant embryos between 48 and 72 hpf revealed that almost no cells divided at such basal positions in controls (Figure 5C). However, in *ath5* morphants, pH3+ cells close to the ILM occurred during the whole span of the experiment, increasing from ~5% of all dividing cells at 48 hpf to ~13% at 72 hpf (Figure 5C). This indicates that the loss of RGCs is at least partially compensated by localized divisions of Ptf1A+ cells. So far, it was assumed that exclusively ACs replenish the RGC layer (Kay et al., 2001). However, we never observed Ptf1A+ divisions giving rise to ACs (Figure 1F; Movie S1). We therefore examined whether cells undergoing extreme basal mitosis in *ath5* morphants represented HC precursors. pH3 immunostaining of Cx55.5:rasGFP embryos revealed that all dividing cells in the prospective RGC layer were indeed Cx55.5+ (Figure 5D; Movie S7). Furthermore, all Cx55.5+ cells in *ath5* morphants were negative for the AC/RGC marker HuC/D (Figure S3B). This suggests that in addition to ACs (Kay et al., 2001), ectopically localized HC precursors contribute to the replenishment of the RGC layer equivalent.

To validate that the loss of RGCs and not the loss of Ath5 itself is responsible for the occurrence of ectopic basal mitoses, we repeated the experiments with a combination of two *ptf1A* morpholinos, which have been demonstrated to suppress HC- and AC-fate decisions (Jusuf et al., 2012). Also upon Ptf1A knockdown, ectopically localized mitoses at basal positions occurred (Figure 5E). Combining *ath5* and *ptf1A* morpholinos (plus *p53* morpholino) resulted in similar ectopic cell divisions (Figure 5F), with Vsx1+ cells dividing close to the ILM. Because Ath5 does not play a role in the determination of the Vsx1 lineage (Jusuf et al., 2011; Vitorino et al., 2009), this confirms that not downregulation of Ath5 itself but loss of neuronal subtypes leads to ectopically localized mitoses of committed precursors.

DISCUSSION

In this study, we performed a systematic analysis of the abundance as well as the mitotic position of different types of precursors during zebrafish retinogenesis. We were able to demonstrate that committed precursors dividing at apical as well as nonapical positions play an unexpectedly prominent role in late retinogenesis. Furthermore, we suggest that morphogenetic constraints and changes in tissue architecture can influence the emergence and position of precursor divisions. Our results are summarized in the model in Figure 4E.

Different Pools of Committed Precursors Displaying Different Morphologies Contribute to Late Zebrafish Retinogenesis

Two distinct pools of nonapically dividing neuronal precursors exist in the zebrafish retina. Sub-apically-dividing Vsx1+ precursors giving rise to two BC daughters appear between 48 and 72 hpf. A second pool of basally dividing HC precursors is seen slightly later, between 56 and 72 hpf. These precursors divide first at the basal side of the INL and later also adjacent to the OPL, giving rise to HCs exclusively. Interestingly, the two different classes of nonapically dividing retinal precursors feature distinct morphologies before and during mitosis. BC precursors lose their apical process upon entry into mitosis but keep their basal process during division. In contrast, HC precursors are nonpolar. Neither of the nonapically dividing cell pools shows a preference for perpendicular division planes. The late phase of apical divisions between 60 and 72 hpf represents not dividing neuroepithelial cells but yet another committed precursor type, namely PR precursors, that feature short, rectangular morphology. While it was suggested that mature PRs are born from apical divisions early in development

(C) An Ath5:gapRFP/Vsx1:GFP (yellow/green) embryo stained for pH3 (magenta) at 56 hpf. Mitoses of Vsx1+ cells occur apically in regions without a complete PR layer (top). In regions with an established PR layer, Vsx1+ divisions are shifted toward subapical locations (bottom). pH3+ cells at the apical side are Ath5+. Scale bar represents 25 μm.

(D) Time-lapse of Vsx1:GFP cells (magenta) transplanted into Ath5:gapRFP (green) background. Vsx1+ cells divide apically in regions without an established PR layer (top, notched arrow). Apical Ath5+ divisions can be observed in regions where PR precursors start to occupy the apical side (middle, filled arrow). Once a compact PR layer is established at the apical side, Vsx1+ divisions occur subapically (bottom, arrow). Time in hr:min. Imaging started at 44 hpf.

(E) Normalized kernel density estimates showing distributions of division locations in control embryos over time (left). Progression of retinal layer formation shown by DAPI staining (right). The emerging groove in the kernel density corresponds to the forming OPL.

If not stated differently, scale bars represent 10 μm. See also Figure S2.

Please cite this article in press as: Weber et al., Mitotic Position and Morphology of Committed Precursor Cells in the Zebrafish Retina Adapt to Architectural Changes upon Tissue Maturation, Cell Reports (2014), http://dx.doi.org/10.1016/j.celrep.2014.03.014

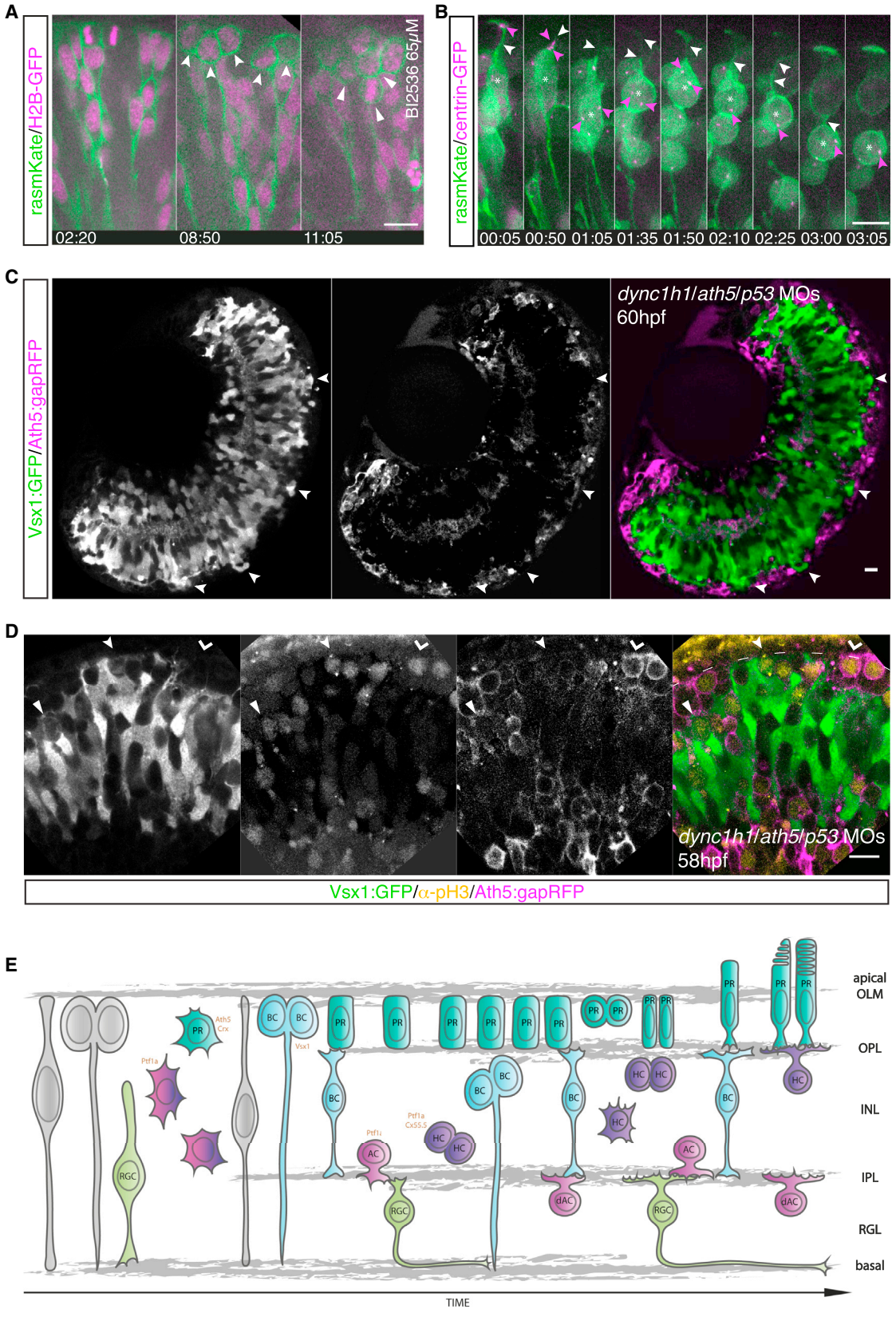

(legend on next page)

(Poggi et al., 2005), these findings show that a high number of apical Ath5+ cells at early stages of retinogenesis resemble immature PR precursors, which divide once more at the apical side.

Committed Precursors Adjust Their Morphology and Mitotic Position According to Architectural Changes Caused by Tissue Maturation

We demonstrate that changes in tissue morphology can influence the mitotic position of committed precursors. In particular, upon the emergence of apical obstacles, precursors undergo mitosis at more basal positions. Apical crowding has previously been suggested to influence neocortex development (Smart, 1972; Okamoto et al., 2013) but is a new concept in retinal development. One striking difference between these two systems is that the offspring of basally dividing progenitors in the neocortex migrate away from their place of birth while daughter cells of basally dividing retinal precursors usually remain within the layer in which they are born. Furthermore, while cortical basal progenitors were shown to correlate with neocortex expansion over evolution (Fietz and Huttner, 2011; Nonaka-Kinoshita et al., 2013), retinal precursors dividing nonapically are most likely a more immediate reaction to increased tissue crowding. For example, development and maturation of the PR layer leads to limited accessibility of the apical space, thereby restricting BC precursor divisions to subapical locations. At the same time, the dividing PR precursors are also affected by the changes that occur upon tissue maturation and therefore adjust their morphology and mitotic position to the remaining apical space.

We conclude that localized divisions of committed precursors are a common phenomenon during late retinogenesis. It is tempting to speculate that such divisions help to enable fast development of retinal layers and at the same time limit migratory distances of cells. Nevertheless, the principle that committed precursor divisions occur exclusively at locations at which the neurons will ultimately polarize and integrate into the network does not always hold true. In the case of HC precursors, a substantial number of divisions occur in the basal INL before cells migrate to their final position adjacent to the OPL. Most likely, a complex mixture of extrinsic and intrinsic factors leads to these seemingly ectopic divisions. For example, it is possible that a further round of cell division is needed to determine HCs, thereby discriminating them from the AC lineage.

Retinal Development Is a Plastic Process Exemplified by the Occurrence of Ectopically Localized Mitoses upon Genetic Ablation of Neuronal Subtypes

We show that retinal development is not always a static and stereotypic process but that ectopic cell divisions can be induced when specific neuronal subtypes fail to develop. Interference with retinal layer formation by genetic depletion of certain cell types leads to the replenishment of these layers by cells of other fates. This replenishment results at least partially from ectopically positioned mitoses of committed precursors. For example, in RGC-depleted *ath5* morphants, Ptf1A+ cells inhabit the most basal layer. This pool of Ptf1A+ cells does not exclusively consist of mispositioned ACs as assumed previously (Kay et al., 2001), but at least a subpopulation represents committed HC precursors undergoing ectopic divisions. This implies that nonapical precursor divisions can be induced in areas in which there is need to compensate for cell loss. It will now be interesting to explore whether local nonapical neurogenesis can also be stimulated upon more general tissue interference, for example by laser ablation along the apicobasal tissue axis. Such experiments will clarify whether more retinal lineages than the ones discussed in this study have the potential to compensate for local cell loss.

At this stage, we are just beginning to explore the underlying causes for the emergence of the different precursors pools dividing at apical, subapical, or basal locations. It is likely that a complex interplay of cell-cell interactions as well as intra- and extracellular signaling cues exists that lead to differences in precursor morphology and position of division. Untangling this plethora of causal factors in the retina and beyond will be an exciting new frontier.

EXPERIMENTAL PROCEDURES

Zebrafish Husbandry

Zebrafish were maintained and bred at 28.5°C. Embryos were raised at 28°C and staged in hpf. Embryos were treated before imaging as described previously (Norden et al., 2009). For immunostaining, embryos were fixed in 4% paraformaldehyde (PFA). All animal work was performed in accordance with European Union directive 2011/63/EU as well as the German Animal Welfare Act.

Figure 4. Correlation between Apical Crowding and Repositioning of Mitotic Cells to Nonapical Locations

(A) The Plk1 inhibitor BI2536 leads to mitotic arrest. Embryos are mosaically injected with rasmKate (green) and H2B-GFP (magenta). Neuroepithelial progenitors translocate their nuclei to the apical side and undergo apical mitosis (left). Cells enter mitosis at the apical side but fail to undergo division, leading to apical accumulation of mitotic cells (notched arrow, middle). Emergence of additional layers of mitotic cells at subapical locations (filled arrow, right); from Movie S6. Time in hr:min. Imaging started at 32 hpf.

(B) Embryos were mosaically injected with rasmKate (green) and centrin-GFP (magenta) and treated with BI2536 (65 μM). A retinal progenitor cannot reach the apical side and enters mitosis subapically (asterisk) upon apical congestion. The apical location of the centrosome is shown (00:05, pink arrows). The centrosome moves toward the nucleus (01:35). The apical process is present at the onset of cell rounding (01:35, white arrows) but lost after centrosome migration (03:05). Time in hr:min. Imaging started at 36 hpf.

(C) Discontinuous PR layer formation in Ath5:gapRFP (magenta) *dync1h1/ath5/p53* morphants (MO). In PR-free areas, Vsx1:GFP (green) cells reach the apical side (arrows).

(D) pH3 staining (yellow) in Vsx1:GFP/Ath5:gapRFP (green/magenta) *dync1h1/ath5/p53* morphant embryos. Vsx1+ divisions are observed subapically in regions with an Ath5+ PR layer (filled arrow) but apically in regions in which the PR layer is disrupted (notched arrow). Apical Ath5+ divisions are observed in regions in which an Ath5+ cell layer forms (kinked arrow).

(E) Model of zebrafish retinogenesis, taking previous data and our findings into account.

Scale bars represent 10 μm. See also Figure S3.

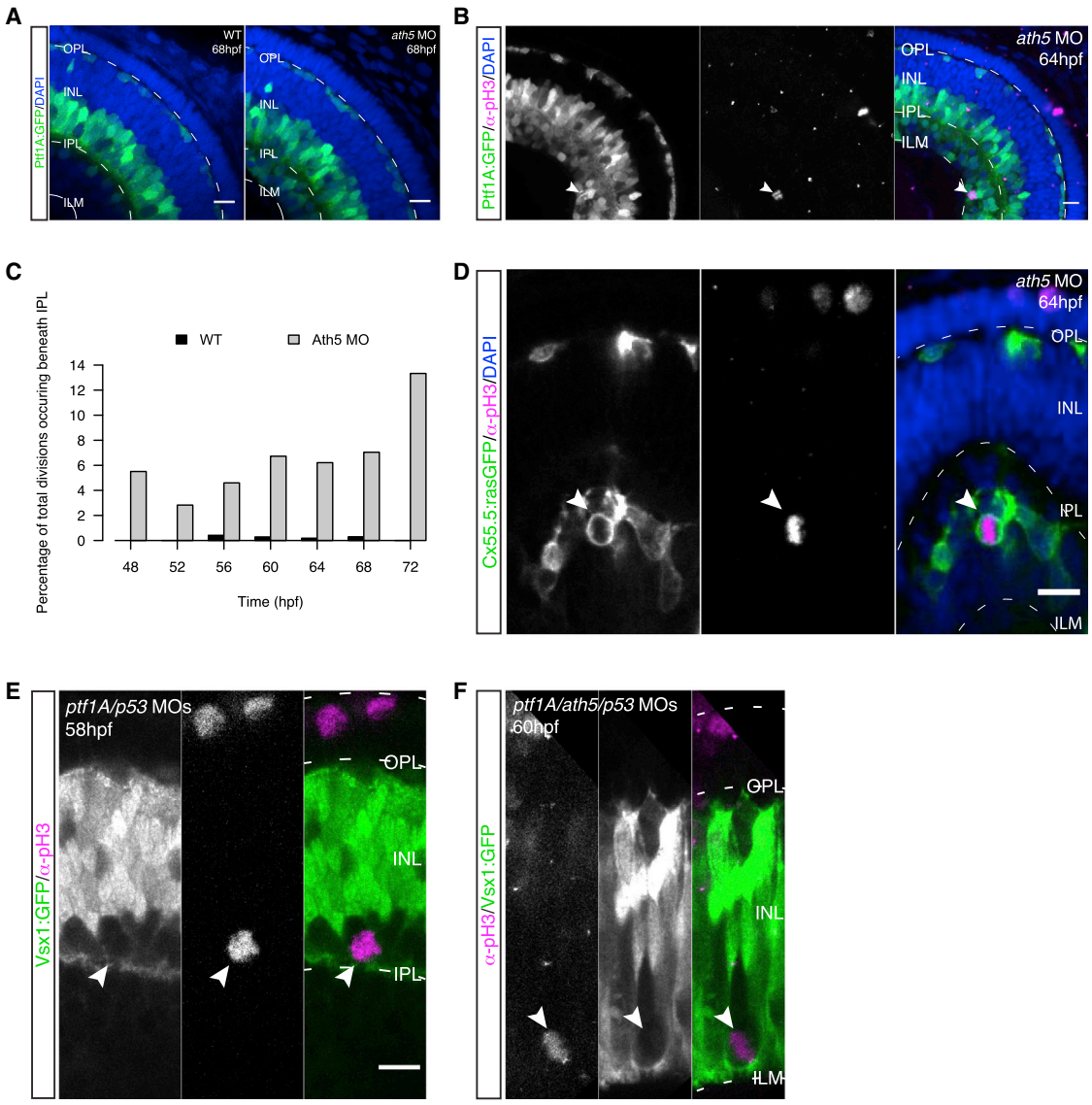

Figure 5. Depletion of Specific Neuronal Subtypes Leads to Ectopic Basal Mitosis of Committed Precursors

(A) Control (left) and *ath5* morphant embryo (MO; right) expressing Ptf1A:GFP (green) and stained for DAPI (blue). In the morphant, the prospective RGC layer is filled with Ptf1A+ cells.

(B) Ptf1A:GFP (green) embryo injected with *ath5* MO and stained for pH3 (magenta) and DAPI (blue). Ptf1A+ division at very basal location (arrows).

(C) Percentage of cell divisions taking place beneath the IPL in control versus *ath5* morphant embryos. Data are pooled from six embryos per time point.

(D) Cx55.5:rasGFP (green) *ath5* morphant embryo stained for pH3 (magenta) and DAPI (blue). pH3+/Cx55.5+ cells are observed underneath the IPL (arrows).

(E) In *ptf1A/ath5/p53* morphants (MO), an ectopic basal division close to the forming IPL occurs. pH3 is shown in magenta, Vsx1:GFP in green, and DAPI in blue.

(F) In *ptf1A/ath5/p53* MO, ectopic Vsx1+ divisions are observed close to the ILM. pH3 is shown in magenta, Vsx1:GFP in green, and DAPI in blue.

Scale bars represent 10 μm. See also Figure S3.

Transgenic Lines and Constructs

Tg(Ptf1a:dsRed) (Vitorino et al., 2009), Tg(Ptf1a:GFP) (Jusuf et al., 2011), Tg(Ath5:gapRFP), Tg(Ath5:gapGFP also known as *atoh7*) (Poggi et al., 2005), and Tg(Vsx1:GFP) (Vitorino et al., 2009) lines have been described previously. Details for the generation of the Tg(Cx55.5:rasGFP) line can be found in Supplemental Experimental Procedures.

RNA and Morpholino Injection and Transplantation

rasGFP, centrin-GFP, H2B-GFP (all in Norden et al., 2009), rasmKate (see Supplemental Experimental Procedures), and Tol2 transposase RNA were synthesized using the Ambion SP6 mMessage Machine kit. RNA was injected into yolk of one-cell stage or into one cell of 16- to 128-cell stage embryos for mosaic expression.

Morpholino sequences can be found in Supplemental Experimental Procedures. The following concentrations were used: *ath5* morpholino, 4 ng per embryo; *ptf1A* morpholinos 1+2, 12 ng each per embryo; *p53* morpholino, 4 ng per embryo; *dync1h1* morpholino, 8 ng per embryo. Morpholinos were obtained from Gene Tools and injected into yolk of one-cell-stage embryos. Transplantations were performed as described elsewhere (Randlett et al., 2013).

Antibodies

Zebrafish whole-mount staining was described previously (Norden et al., 2009). A list of all antibodies used can be found in Supplemental Experimental Procedures. Nuclei were stained with DAPI.

Image Acquisition and Analysis

For live imaging, optical sections were 1 μm. Embryos were mounted in 1% low-melt agarose in E3 medium on Mattek glass-bottom dishes. An Andor spinning disk system with an Olympus UPlanSApo 60× water-immersion objective (numerical aperture [NA] = 1.2) was used at 30°C. Image analysis was performed using ImageJ/Fiji software (National Institutes of Health).

For statistical analysis of fixed samples, embryos were fixed (4% PFA) every 4 hr from 36 to 76 hpf and stained for pH3 and DAPI. Retinae of two to six embryos per time point were analyzed. Imaging was performed on a Zeiss Axiovert 200M with a Zeiss C-Apochromat 63× water-immersion objective (NA = 1.2) or on a Zeiss LSM 710 NLO with a Zeiss LD C-Apochromat 40× water-immersion objective (NA = 1.1). Optical sagittal sections of the central retina were taken and the center (in z) of the retina was defined as the optical center of each stack. A total of 15 μm above and below this center were acquired. Mitotic cells in *ath5* morphants versus control embryos were counted in stacks of 15 μm (for embryos between 48 and 60 hpf) or 30 μm (for embryos between 64 and 72 hpf).

To analyze the effect of RGC ablation on the occurrence of nonapically dividing precursors, distances of dividing cells from the apical surface were plotted. The proportion of cells dividing beneath the IPL was calculated by measuring IPL location at each time point.

BI2536 Drug Treatment

For details on BI2536 drug treatment, please see the Supplemental Experimental Procedures.

SUPPLEMENTAL INFORMATION

Supplemental Information includes Supplemental Experimental Procedures, three figures, and seven movies and can be found with this article online at http://dx.doi.org/10.1016/j.celrep.2014.03.014.

ACKNOWLEDGMENTS

We thank F. Calegari, P. Jusuf, M. Karl, I. Kelava, J. Rink, M. Thompson, the C.N. lab, W.A. Harris, and F. Jug for helpful comments. Special thanks go to A.M. Sykes. R. Wong shared the Cx55.5 construct. C. Froeb, the MPI-CBG fish facility, and the Light Microscopy Facility are thanked for experimental help. I.P.W. and P.J.S. are members of the DIGS-BB PhD program. A.P.R. was supported by an Erasmus grant. C.N. is supported by an HFSPO Career Development Award and the German Research Foundation (DFG) (SFB 655, A25).

Received: May 20, 2013
Revised: January 13, 2014
Accepted: March 5, 2014
Published: April 3, 2014

REFERENCES

Agathocleous, M., and Harris, W.A. (2009). From progenitors to differentiated cells in the vertebrate retina. Annu. Rev. Cell Dev. Biol. *25*, 45–69.

Boije, H., Edqvist, P.-H.D., and Hallböök, F. (2009). Horizontal cell progenitors arrest in G2-phase and undergo terminal mitosis on the vitreal side of the chick retina. Dev. Biol. *330*, 105–113.

Del Bene, F., Wehman, A.M., Link, B.A., and Baier, H. (2008). Regulation of neurogenesis by interkinetic nuclear migration through an apical-basal notch gradient. Cell *134*, 1055–1065.

Fietz, S.A., and Huttner, W.B. (2011). Cortical progenitor expansion, self-renewal and neurogenesis-a polarized perspective. Curr. Opin. Neurobiol. *21*, 23–35.

Godinho, L., Williams, P.R., Claassen, Y., Provost, E., Leach, S.D., Kamermans, M., and Wong, R.O.L. (2007). Nonapical symmetric divisions underlie horizontal cell layer formation in the developing retina in vivo. Neuron *56*, 597–603.

Gomes, F.L.A.F., Zhang, G., Carbonell, F., Correa, J.A., Harris, W.A., Simons, B.D., and Cayouette, M. (2011). Reconstruction of rat retinal progenitor cell lineages in vitro reveals a surprising degree of stochasticity in cell fate decisions. Development *138*, 227–235.

He, J., Zhang, G., Almeida, A.D., Cayouette, M., Simons, B.D., and Harris, W.A. (2012). How variable clones build an invariant retina. Neuron *75*, 786–798.

Hu, M., and Easter, S.S. (1999). Retinal neurogenesis: the formation of the initial central patch of postmitotic cells. Dev. Biol. *207*, 309–321.

Insinna, C., Baye, L.M., Amsterdam, A., Besharse, J.C., and Link, B.A. (2010). Analysis of a zebrafish dync1h1 mutant reveals multiple functions for cytoplasmic dynein 1 during retinal photoreceptor development. Neural Dev. *5*, 12.

Jusuf, P.R., Almeida, A.D., Randlett, O., Joubin, K., Poggi, L., and Harris, W.A. (2011). Origin and determination of inhibitory cell lineages in the vertebrate retina. J. Neurosci. *31*, 2549–2562.

Jusuf, P.R., Albadri, S., Paolini, A., Currie, P.D., Argenton, F., Higashijima, S.I., Harris, W.A., and Poggi, L. (2012). Biasing amacrine subtypes in the Atoh7 lineage through expression of Barhl2. J. Neurosci. *32*, 13929–13944.

Kay, J.N., Finger-Baier, K.C., Roeser, T., Staub, W., and Baier, H. (2001). Retinal ganglion cell genesis requires lakritz, a Zebrafish atonal Homolog. Neuron *30*, 725–736.

Lee, H.O., and Norden, C. (2013). Mechanisms controlling arrangements and movements of nuclei in pseudostratified epithelia. Trends Cell Biol. *23*, 141–150.

Lénárt, P., Petronczki, M., Steegmaier, M., Di Fiore, B., Lipp, J.J., Hoffmann, M., Rettig, W.J., Kraut, N., and Peters, J.-M. (2007). The small-molecule inhibitor BI 2536 reveals novel insights into mitotic roles of polo-like kinase 1. Curr. Biol. *17*, 304–315.

Leung, L., Klopper, A.V., Grill, S.W., Harris, W.A., and Norden, C. (2011). Apical migration of nuclei during G2 is a prerequisite for all nuclear motion in zebrafish neuroepithelia. Development *138*, 5003–5013.

Livesey, F.J., and Cepko, C.L. (2001). Vertebrate neural cell-fate determination: lessons from the retina. Nat. Rev. Neurosci. *2*, 109–118.

Ma, W., Yan, R.T., Xie, W., and Wang, S.Z. (2004). A role of ath5 in inducing neuroD and the photoreceptor pathway. J. Neurosci. *24*, 7150–7158.

Nonaka-Kinoshita, M., Reillo, I., Artegiani, B., Martínez-Martínez, M.Á., Nelson, M., Borrell, V., and Calegari, F. (2013). Regulation of cerebral cortex size and folding by expansion of basal progenitors. EMBO J. *32*, 1817–1828.

Norden, C., Young, S., Link, B.A., and Harris, W.A. (2009). Actomyosin is the main driver of interkinetic nuclear migration in the retina. Cell *138*, 1195–1208.

Okamoto, M., Namba, T., Shinoda, T., Kondo, T., Watanabe, T., Inoue, Y., Takeuchi, K., Enomoto, Y., Ota, K., Oda, K., et al. (2013). TAG-1-assisted progenitor elongation streamlines nuclear migration to optimize subapical crowding. Nat. Neurosci. *16*, 1556–1566.

Passini, M.A., Levine, E.M., Canger, A.K., Raymond, P.A., and Schechter, N. (1997). Vsx-1 and Vsx-2: differential expression of two paired-like homeobox genes during zebrafish and goldfish retinogenesis. J. Comp. Neurol. *388*, 495–505.

Perkins, B.D., and Fadool, J.M. (2010). Photoreceptor structure and development: analyses using GFP transgenes. Methods Cell Biol. *100*, 205–218.

Pittman, A.J., Law, M.Y., and Chien, C.B. (2008). Pathfinding in a large vertebrate axon tract: isotypic interactions guide retinotectal axons at multiple choice points. Development *135*, 2865–2871.

Poggi, L., Vitorino, M., Masai, I., and Harris, W.A. (2005). Influences on neural lineage and mode of division in the zebrafish retina in vivo. J. Cell Biol. *171*, 991–999.

Randlett, O., MacDonald, R.B., Yoshimatsu, T., Almeida, A.D., Suzuki, S.C., Wong, R.O., and Harris, W.A. (2013). Cellular requirements for building a retinal neuropil. Cell Rep *3*, 282–290.

Please cite this article in press as: Weber et al., Mitotic Position and Morphology of Committed Precursor Cells in the Zebrafish Retina Adapt to Architectural Changes upon Tissue Maturation, Cell Reports (2014), http://dx.doi.org/10.1016/j.celrep.2014.03.014

Sernagor, E., Eglen, S., Harris, W.A., and Wong, R.O. (2006). Retinal Development, 1st Edition (Cambridge: Cambridge University Press).

Shields, C.R., Klooster, J., Claassen, Y., Ul-Hussain, M., Zoidl, G., Dermietzel, R., and Kamermans, M. (2007). Retinal horizontal cell-specific promoter activity and protein expression of zebrafish connexin 52.6 and connexin 55.5. J. Comp. Neurol. *501*, 765–779.

Smart, I.H. (1972). Proliferative characteristics of the ependymal layer during the early development of the mouse diencephalon, as revealed by recording the number, location, and plane of cleavage of mitotic figures. J. Anat. *113*, 109–129.

Suzuki, S.C., Bleckert, A., Williams, P.R., Takechi, M., Kawamura, S., and Wong, R.O. (2013). Cone photoreceptor types in zebrafish are generated by symmetric terminal divisions of dedicated precursors. Proc. Natl. Acad. Sci. USA *110*, 15109–15114.

Turner, D.L., Snyder, E.Y., and Cepko, C.L. (1990). Lineage-independent determination of cell type in the embryonic mouse retina. Neuron *4*, 833–845.

Vitorino, M., Jusuf, P.R., Maurus, D., Kimura, Y., Higashijima, S.-I., and Harris, W.A. (2009). Vsx2 in the zebrafish retina: restricted lineages through derepression. Neural Dev. *4*, 14.